Applied Catalysis B: Environmental 259 (2019) 118070

Contents lists available at ScienceDirect

Applied Catalysis B: Environmental

journal homepage: www.elsevier.com/locate/apcatb

Synergistic effects of bimetallic PtRu/MCM-41 nanocatalysts for glycerol oxidation in base-free medium: Structure and electronic coupling dependent activity

Hao Yan, Shuang Yao, Bin Yin, Wei Liang, Xin Jin, Xiang Feng, Yibin Liu*, Xiaobo Chen, Chaohe Yang*

State Key Laboratory of Heavy Oil Processing, China University of Petroleum, Qingdao 266580, China

ARTICLE INFO

Keywords:
Bimetallic PtRu
MCM-41
Glycerol oxidation
DFT

ABSTRACT

Bimetallic PtRu catalyst was first reported for oxidation of glycerol to glyceric acid in base-free medium using O_2 as the oxidant. A combination of density functional theory (DFT) calculations and multi-characterizations (e.g., H_2-TPR, HAADF-STEM and XPS) revealed that the strong interaction between Pt and Ru could promote the dispersion of PtRu alloy nanoparticles and enhance the electronic coupling effect on the metal surface. Meanwhile, compared to the monometallic Pt catalyst, the introduction of Ru contributes to the direct dissociation of molecular oxygen and water to hydroxyl group, leading to the excellent catalytic activity. A volcanic-shaped relationship between Ru/Pt ratio, catalytic performance, structure-sensitivity and electronic coupling effect was systematically established. Furthermore, the role of structure-sensitivity and electronic coupling effect for the enhanced catalytic activity of PtRu catalysts with different Ru/Pt ratios are distinguished in detail. Finally, the $Pt_{0.8}Ru_{0.8}$/MCM-41 catalyst showed excellent catalytic activity (TOF: 823.9 h^{-1}), glyceric acid selectivity (80.1%) and stability (recycling for 5th) under the optimized conditions (80 °C, 1 MPa O_2 and 12 h). The insights and methodology reported here may pave the way to the rational design of bimetallic catalysts for efficient conversion of bio-derived substrates under mild conditions.

1. Introduction

Recently, developing smart technologies to realize the comprehensive utilization of biomass, as an environmentally and sound resource, has attracted much attention [1–3]. In this scenario, the concept of bio-refinery emerged. Briefly, bio-refinery is to transform various biomass components including cellulose, hemicellulose, lipids, lignin and chitin into high value-added chemicals (such as glycol, carboxylic acid, amino acid, nitriles and pyrrole) via a number of catalytic processes [4–10]. Glycerol (GLY) is a critical building block in bio-refinery because the production of biodiesel could generate a lot of inexpensive glycerol as a by-product [11,12]. Compared to other procedure (such as transesterification, dehydration, esterification, hydrogenolysis and polymerization), oxidation of GLY under mild conditions is an attractive way since GLY-derived oxidation products could serve various substrates for the manufacture of high-end chemicals [13,14].

Glycerol oxidation, which is a sequential reaction that follows multiple paths, could generate various products such as dihydroxyacetone (DHA), hydroxypyruvic acid (HYPAC), glyceric acid (GLYA), glyceraldehyde (GLYAD), and glycolic acid (GLYOA) [15]. Therefore, the development of highly active, selective and stable catalysts is necessary to achieve the desired compound. DHA is an important product due to its application in cosmetics fine chemicals industry [16,17]. The generation of DHA via catalytic oxidation of GLY has also been largely studied using iron zeolites [14] and the bimetallic catalysts such as Pt-Bi [17], Pt-Sb [18] and Pd-Ag [19]. GLYA is another desirable intermediate for the generation of other deeply oxidized products such as mesoxalic acid and tartronic acid [20,21]. Typically, Au, Pd and Pt nanocatalysts were reported. However, excessive amount of soluble base additives (*i.e.*, NaOH) must be added to obtain a high yield of GLYA, as it is well know that the soluble base facilitates O—H bond activation and alkoxide formation in the oxidation of alcohols [11]. In addition, the soluble base could prevent the metal leaching via the generation of carboxylate instead of acid [12]. The oxidation of aldehyde (−CHO) to carboxylic acid (−COOH) could proceed smoothly in the presence of a base [10]. Actually, GLYA in the form of a salt needs the extra acidification and purification resulting in the lower green process and higher application cost [15]. Therefore, the selective

* Corresponding author.
E-mail address: liuyibin@upc.edu.cn (Y. Liu).

https://doi.org/10.1016/j.apcatb.2019.118070
Received 9 May 2019; Received in revised form 23 July 2019; Accepted 7 August 2019
Available online 08 August 2019
0926-3373/

oxidation of GLY in base-free medium is an ideal route [10], while developing efficient catalysts still remains significant challenges.

Recent advances have been achieved on various supported Pt-based catalysts [22,23]. It is found that the properties of support materials, which are combined with noble metal, played an important role in realizing the oxidation of GLY in base-free medium via different mechanism [20]. Solid bases (such as magnesium oxide and hydrotalcite) and surface functionalized carbon materials (such as carbon nanofibers, reduced grapheme oxide and MWNTs) were frequently employed as supports [12,24–27]. However, limited improvement in the activity and selectivity has been achieved by changing the properties of supports. After Liu and co-workers first reported the Au-Pt catalyst for glycerol oxidation [28], more efficient Pt-based bimetallic catalysts have been developed. By alloying the second metal (such as Au [28], Ni [29], Cu [30] and Sn [8]) with Pt, the catalytic performance has been significantly improved. The selectivity of GLYA on bimetallic PtCo catalysts (85.9%) was higher than that on monometallic Pt catalyst [24]. In addition, the activity and stability of catalysts could be simultaneous improved on PtAu and PtSn catalysts. However, it remains challenging to prepare Pt based nanocatalysts on unmodified supports together with high activity, high selectivity and superior stability for the oxidation of GLY to GLYA.

As the least expensive noble metal, Ru is worth exploring and limited catalyst candidates have been explored. Monometallic Ru catalyst has exhibited exceptional performances in 5-hydroxymethylfurfural base-free aerobic oxidation [1]. Bimetallic Au-Ru supported on ceria-zirconium mixed oxide exhibited stable catalytic performances for GLY oxidation under alkaline conditions because the presence of small amounts of Ru could prevent the aggregation of gold particles [31]. Besides, there is no literature about GLY oxidation on Ru-based catalysts under alkaline or non-alkaline conditions. Bimetallic PtRu catalysts have proven to be very effective for methanol, ethylene glycol and glycerol electrooxidation, offering significantly increased currents at low potentials relative to pure Pt [32–35]. The electrooxidation mechanism of alcohols is somewhat similar to that of glycerol oxidation, both of which need the dissociation of water (with oxygen) and dehydrogenation oxidation [32]. In addition, the incorporation of Ru to Pt could weaken the adsorption of both C═O and O—H bonds on the Pt sites, while the bonds of these species on the Ru sites are strengthened [36]. Interestingly, the GLY oxidation was inhibited by the strong adsorption of ketone intermediates and condensation products of ketones, which could cover the active sites leading to the deactivation of Pt catalysts [37]. These indicate that bimetallic PtRu catalysts have potential as a stable and efficient catalyst for GLY oxidation.

In this work, we report bimetallic PtRu/MCM-41 catalysts for selective oxidation of glycerol to glyceric acid without a liquid base for the first time. The proposed PtRu catalysts immobilized on MCM-41 support were prepared via co-impregnation method, and the underlying structure-performance relationship was systematically elucidated by multi-characterizations (e.g., H_2-TPR, H_2-TPD, CO-TPD, HAADF-STEM, TEM-EDX, HRTEM, XPS, XRD, N_2-physisorption, ICP-OES) and DFT calculation. The introduction of Ru significantly enhances the catalytic activity (up to 823.9 h^{-1}), improves the selectivity of glyceric acid (up to 80.1%) and strengthen the catalyst stability (recycling for 5 times). The PtRu/MCM-41 catalysts have small nanoparticles and stronger interaction between Pt and Ru atoms. The enhanced electron transfer ability promotes the direct dissociation of molecular oxygen and water to OH group, resulting in the excellent catalytic performance. In addition, the relationship between Ru/Pt ratio and catalytic activity is further investigated. The multi-methodology (experimental characterization methods together with DFT calculation) could provide basic principles for the rational design of other efficient bimetallic catalysts in the process of biomass conversion.

2. Experimental

2.1. Chemicals

Hexadecyl trimethyl ammonium bromide (CTAB, 99%) and tetraethyl orthosilicate (TEOS, 98%) were provided by Sigma-Aldrichk. Ruthenium(III) chloride hydrate ($RuCl_3{\cdot}xH_2O$, 35–42% Ru basis), ammonia solution tetrahydrate ($NH_3{\cdot}H_2O$, 25%–28%) and chloroplatinic acid ($H_2PtCl_6{\cdot}6H_2O$, (99.9% ACS, Pt min 37.5%)) were provided by Sinopharm Chemical Reagent Co.,Ltd.

2.2. Catalyst preparation

Mesoporous MCM-41 materials were prepared by hydrothermal synthesis [38]. A typical procedure is described as follows. 2.7 g of CTAB was dissolved in 125 mL water (35 °C) with stirring, followed by the addition of 33 mL $NH_3{\cdot}H_2O$. When the color of the solution became clear, 14 mL of TEOS was added to obtain a homogeneous mixture. After 30 min agitation, the resulting gel was transferred to a 200 mL autoclave and aged to 110 °C for 52 h. Finally, the mixture was filtered, dried under 100 °C and calcined at 550 °C in air for 6 h. MCM-41 (80 °C) and MCM-41 (140 °C) samples were prepared at the crystallization temperature of 80 °C and 140 °C, respectively [39]. To further enlarge the pore size, MCM-41 (6 days) sample was prepared by prolonging crystallization time to 6 days at 140 °C [39].

Supported Pt, Ru and PtRu catalysts were prepared by incipient impregnation with $RuCl_3{\cdot}xH_2O$ solution. The catalysts with different Ru loadings were labeled as $Pt_{0.8}Ru_{0.4}$/MCM-41, $Pt_{0.8}Ru_{0.8}$/MCM-41, $Pt_{0.8}Ru_{1.2}$/MCM-41 and $Pt_{0.8}Ru_{1.6}$/MCM-41. The Pt loading of the catalysts was 0.8 wt%. The loading of Pt/MCM-41 and Ru/MCM-41 catalysts are 0.8 wt% and 1.6 wt% respectively. $Pt_{0.8}Ru_{1.6}$/MCM-41 (Mix) catalyst was obtained by mechanical mixing of Pt/MCM-41 and Ru/MCM-41 catalysts.

2.3. Catalyst characterization

X-ray diffraction patterns (XRD) of PtRu/MCM-41 samples were measured on X'pert PRO MPD diffractometer. The PtRu loadings were determined by the inductive coupled plasma optical emission spectrometry (ICP-OES) and the N_2 adsorption-desorption isotherms were determined on a Micromeritics ASAP 2020 instrument. JEOL JSM-2010 instrument was used to take the high-resolution transmission electron microscopy (HRTEM) images. A Tecnai G2 F20 S-Twin equipped with a digitally processed STEM imaging system was used to take high-angle annular dark-field scanning transmission electron microscopy (HAADF-STEM) images. Valence states and composition of surface metals were measured by X-ray photoelectron spectroscopy (XPS). Micromeritics AutoChemII2920 system was used to conduct the H_2 temperature-programmed reduction (H_2-TPR). In a typical process, unreduced catalyst sample (ca. 100 mg) was reduced in flowing gas containing 10 vol.% H_2 in Ar (50 mL/min), and using a heating rate of 15 K/min up to a final temperature of 1073 K. The H_2 (or CO)-TPD on the reduced catalyst was also used the Micromeritics AutoChemII2920 system. It was hypothesized that the amount of chemisorbed and desorbed H_2 (or CO) were equal. All the samples could be initially reduced by H_2 for 1 h. Then, the reactor was cooled to 323 K, and held at this temperature for 0.5 h to eliminate the weakly bound physisorbed H_2 of the sample. Subsequently, the temperature of the sample was ramped to 773 K (10 K/min) and held for 0.5 h. The effluent gas was observed by the TCD and a H_2 (or CO)-TPD profile could be obtained in the process of temperature of ramp.

2.4. Glycerol oxidation

In a typical evaluation of catalysts performance, 0.2 g catalyst and 25 mL glycerol solution (0.22 M) were added into a 50 mL autoclave.

Firstly, the reactor was purged twice by pure O_2. Then, it was heated to 80 °C and held for 8 h at a stirring rate of 1000 rpm. After the reaction, the samples were analyzed using a Shimadzu HPLC LC-20AT with two detectors [refractive index (RID-10A) and UV(SPD-20A)]. The definition of conversion, selectivity and turn over frequency (TOF) have been described in other literatures [32,38,39].

2.5. Density functional theory (DFT) calculations

All DFT calculations had been done using DMol^3 program package [40]. The Perdew-Burke-Ernzerhof (PBE) approximation based on the generalized gradient approximation (GGA) was selected to calculate the potential energy surface of oxidation reactions on the metal surface [32,40–43]. It has been demonstrated that the inclusion of vdW interaction by using TS's DFT-D2 method for reaction substrates and products involved in the reaction on various metal surfaces (such as Cu, Ru, Pd, and Pt) [42]. The effective core potential (ECP) method was selected for the Ru and Pt atoms, and spin unrestricted was selected.

The 1:1 PtRu(111) alloy was used as the computational model for the oxidation catalysts [32]. A periodic four-layer slab containing a vacuum of 18 Å in thickness and a 4 × 4 unit cell was established. This PtRu model has been widely accepted in the oxidation reactions [36]. The density of Monkhorst-Pack scheme k-point of 3 × 3 × 1 were chosen [12,44]. The atoms which located in the two bottom layers were fixed. The transition state (TS) was completely searched by the linear/quadratic synchronous transit (LST/QST) method [40,45]. Moreover, the TS has only one imaginary frequency. Zero-point energy corrections were introduced to correct the energies of reactants, transition states (TS), and products [46]. All the adsorption energies are defined as follows:

$$E_a = E_{ads+cat} - E_{ads} - E_{cat}$$

E_a, $E_{ads+cat}$, E_{ads} and E_{cat} represent the adsorption energy of adsorbate on the metal surface, the total energy of the slab with an adsorbed molecule, the energies of the free adsorbate and the clean slab, respectively.

3. Results and discussion

3.1. Enhanced catalytic performance for the PtRu/MCM-41 catalysts

The Ru/MCM-41, Pt/MCM-41, $Pt_{0.8}Ru_{1.6}$/MCM-41 (Mix) and $Pt_{0.8}Ru_{0.8}$/MCM-41 catalysts were prepared by impregnation method and tested for the GLY oxidation using molecular O_2 as the oxidant at 80 °C and 1 MPa O_2. The composition and metal dispersion of these catalysts are provided in Table S1. The metal dispersion was measured from TEM images for the relative accuracy of the turnover frequency (TOF), which was then calculated as mole of GLY converted per mole of surface Pt atoms per hour. When the conversion was no more than 10%, the average reaction rate is approximately equal to the instantaneous reaction rate. As shown in Fig. 1, the Ru/MCM-41 catalyst is almost inactive for the GLY oxidation. In contrast, the introduction of Ru greatly enhances the TOF from 328.1 to 823.9 h^{-1}. This clearly shows the promotional effect of Ru. Meanwhile, the catalytic performance of the $Pt_{0.8}Ru_{1.6}$/MCM-41 (Mix) catalyst is even worse than that of the Pt/MCM-41 catalyst. The $Pt_{0.8}Ru_{0.8}$/MCM-41 catalyst exhibits excellent activity (TOF: 823.9 h^{-1}) and selectivity of GLYA (74.1%) in base-free medium, indicating that the structure formed between Pt and Ru promotes GLY oxidation. Preliminary results on bimetallic $Pt_{0.8}Ru_{0.8}$/MCM-41 catalyst motivated us to further investigate the structure–activity and electronic coupling effect relations during the oxidation of GLY to GLYA.

The physico-chemical properties of the Ru/MCM-41, Pt/MCM-41, $Pt_{0.8}Ru_{1.6}$/MCM-41 (Mix) and $Pt_{0.8}Ru_x$/MCM-41 catalysts were analyzed to elucidate the intrinsic reason for the distinct catalytic performance. H_2-TPR was first employed to characterize the reduction

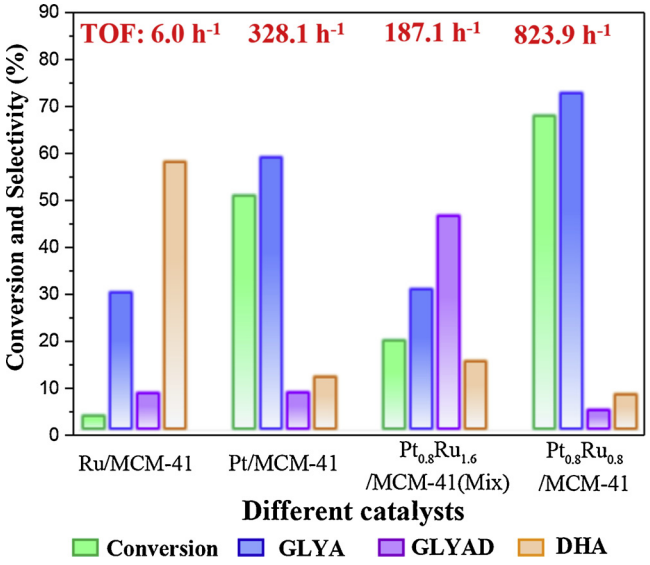

Fig. 1. Catalytic performances of the Ru/MCM-41, Pt/MCM-41, $Pt_{0.8}Ru_{1.6}$/MCM-41 (Mix) and $Pt_{0.8}Ru_{0.8}$/MCM-41 catalysts in glycerol oxidation (experimental conditions: 25 mL aqueous solution of glycerol (0.22 M) 0.2 g solid catalysts, 8 h).

properties of catalysts. Since the catalyst loading is relatively low, the 200-500 °C TCD signal is amplified and plotted in Fig. 2b. As shown in Fig. 2, the monometallic Ru/MCM-41 catalyst exhibits two reduction peaks at ~134 °C and ~318 °C, revealing the reduction of RuO_x to Ru [47]. The monometallic Pt/MCM-41 catalyst shows a reduction peaks at ~ 297 °C corresponding to the reduction of PtO_x to Pt [48]. The negative peak at ~ 80 °C is attributed to desorption of H_2 on the surface of Pt [49]. The PtRu/MCM-41 catalysts show two peaks at ~140 °C and 310 °C. As the Ru loading increases to 0.8 wt% (Fig. 2b), these two peaks shift to higher temperature, suggesting a strong interaction between Pt and Ru atoms [50]. The reduction temperature (~350 °C) is sufficient to completely transform the metal oxide to the zero-valent state for both Ru and Pt. Ruiz et al [50]. demonstrated that the identical result is related to the co-crystallization of Ru and Pt chlorides in the drying procedure of the preparation. Therefore, it is possible to form PtRu alloys in the $Pt_{0.8}Ru_x$/MCM-41 catalysts. The $Pt_{0.8}Ru_{1.6}$/MCM-41 (Mix) catalyst does not exhibit such characteristic, suggesting that PtRu bimetallic is not a simple physical interaction. In addition, excessive Ru does not further increase the reduction temperature, thus only appropriate PtRu ratio could enhance the metal interaction.

Table 1 shows the metallic dispersion and surface atoms determined by H_2-TPD and CO-TPD for the PtRu/MCM-41 catalysts. It is found that the monometallic Pt/MCM-41 catalyst displays the highest metal dispersion and highest capacity for H_2 adsorption [51]. Due to the well-established character of activated H_2 on the Ru nanoparticles, the Ru/MCM-41 catalyst displays much lower adsorption ability for H_2 than CO [51,52]. With the increase of Ru content, the metal dispersion (measured by H_2-TPD) of the PtRu/MCM-41 catalysts decreases. More importantly, the amount of adsorbed H_2 on the surface decreases with incorporation of Ru, indicating that the active sites of Pt on the surface decrease gradually. At a Ru/Pt ratio of 1, the amount of adsorbed H_2 on the surface decreases to approximately half of the original amount. The metal dispersion measured by CO-TPD does not exhibit a progressive correlation with the content of Ru. It has been reported that the Ru sites could be covered by CO, while the adsorption ability of CO on Pt is reduced in the PtRu alloy structure [51,52]. Therefore, the difference tendencies in H_2 and CO adsorption for the PtRu/MCM-41 catalysts can be attributed to the formation of PtRu alloy structure.

HAADF-STEM was employed to determine the size distribution of metal nanoparticles on Pt-Ru catalysts. As shown in Fig. 3a-f, all the

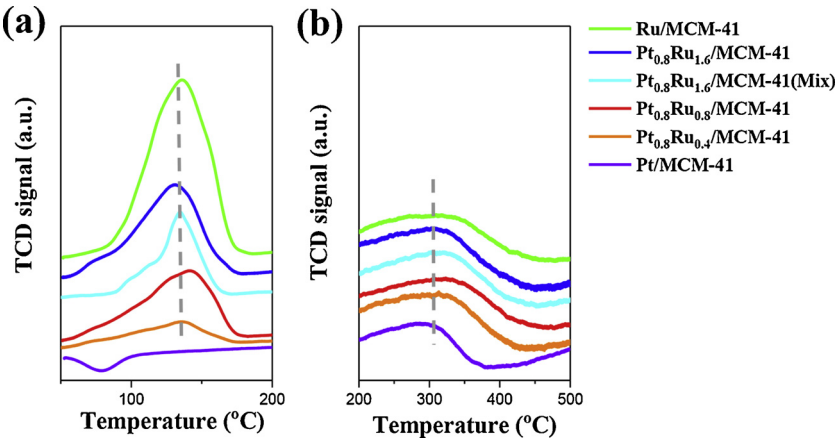

Fig. 2. H_2-TPR profiles of Ru/MCM-41, Pt/MCM-41, $Pt_{0.8}Ru_{1.6}$/MCM-41 (Mix) and $Pt_{0.8}Ru_x$/MCM-41 catalysts.

catalysts display well-dispersed and uniform metal nanoparticles. The $Pt_{0.8}Ru_{0.8}$/MCM-41 catalyst has smaller average metal particle size (ca. 2.1 nm) than Pt/MCM-41 (ca. 3.7 nm) and Ru/MCM-41 (ca. 3.0 nm) catalysts, indicating that the incorporation of Ru promotes the dispersion of Pt [33]. It has been demonstrated that the smaller Pt nanoparticles are more active in the GLY oxidation [27]. Therefore, the smaller nanoparticle size of $Pt_{0.8}Ru_{0.8}$/MCM-41 catalyst could be one reason for the enhanced TOF. In addition, the particle size decreases with the incorporation of Ru in the initial stage. When the loading of Ru is higher than 0.8 wt%, the particle size increases slightly due to the high metal loading ($Pt_{0.8}Ru_{1.2}$/MCM-41 catalyst: 2.3 nm; $Pt_{0.8}Ru_{1.6}$/MCM-41 catalyst: 2.6 nm). It further indicates that there is an optimal ratio in the PtRu alloy.

TEM-EDX and HRTEM of the $Pt_{0.8}Ru_{0.8}$/MCM-41 catalyst were further investigated. EDX mapping in Fig. 4a clearly shows that Pt and Ru species are well dispersed on the MCM-41 support and the Ru is present along with Pt, indicating the formation of Pt-Ru alloy nanoparticle in the $Pt_{0.8}Ru_{0.8}$/MCM-41 catalyst. The structure of Pt-Ru nanoparticles was further studied by HRTEM. As shown in Fig. 4b, the lattice spacing of Pt-Ru nanoparticles is approximately 0.217 nm, which is smaller than that of Pt (111) (ca. 0.227 nm) and larger than that of Ru (0002) (ca. 0.210 nm) [53,54]. This indicates that the growth of Pt lattice planes is clearly disturbed by Ru due to large lattice constant mismatch between the Pt and Ru (Pt: 0.39 nm; Ru: 0.27 nm) [55]. Jin et al. [55] found that anisotropic growth induced by lattice mismatch could contribute to the final nanocrystal geometry resulting in the unusual electronic coupling and a synergistic enhancement in catalytic oxidation reaction. Therefore, the PtRu alloy nanoparticles enhanced the catalytic performance of the $Pt_{0.8}Ru_{0.8}$/MCM-41 catalyst in the GLY oxidation.

The structure of PtRu/MCM-41 catalysts was then studied by XRD and N_2-physisorption. All the catalysts exhibit typical structure of MCM-41 with high crystallinity (Fig. S1). No obvious peaks ascribing to Pt nanoparticle can be observed in high-angle of XRD because of the uniform nanoparticle distribution and low metal loading of Pt. When the metal loading of Ru increases, the characteristic peaks of metal Ru appear at ~ 38.3, 41.9 and 43.7° [56]. Moreover, the characteristic peaks of bimetallic $Pt_{0.8}Ru_x$/MCM-41 catalysts shift to a lower angle than that of Ru/MCM-41 catalyst. The lattice stretching could be attributed to the formation of PtRu alloy nanoparticles [57]. Subsequently, N_2-physisorption measurement also reveals the typical type-IV isotherm of MCM-41 mesoporous materials (Fig. S2) [58]. The large surface area and regular pore structure of the inert MCM-41 support could promote the dispersion of metal nanoparticles. There is a certain reduction of pore volume and surface area for the PtRu/MCM-41 catalysts after the embedding of Pt and Ru metals (Table S2). But all the catalysts still display a relatively high specific surface area and pore volume, which could provide uniform active sites for the oxidation reaction.

The bimetallic PtRu/MCM-41 catalysts were further characterized using XPS and DFT calculation to investigate the surface metal valence state, metal-metal coupling effect and possible reconfiguration of surface electrons. In Fig. 5(a-1), the binding energy of Pt $4f_{7/2}$ for the Pt/MCM-41 catalyst is 71.3 eV. With the incorporation of Ru, the separated spin-orbits of Pt $4f_{5/2}$ and Pt $4f_{7/2}$ shift to lower binding energy, indicating that Pt obtains electrons [54]. Specifically, the $Pt_{0.8}Ru_{0.8}$/MCM-41 catalyst displays lowest binding energy of Pt $4f_{7/2}$ (70.9 eV). In contrast, excessive Ru increases the binding energy of Pt 4f, suggesting that there is an appropriate ratio between Pt and Ru. To get rid of the overlapping between Ru 3*d* and C1*s* regions, the Ru 3*p* region is usually examined. Fig. 5(a-2) shows that the Ru/MCM-41 catalyst displays lowest binding energy of Ru $3p_{3/2}$ (460.8 eV). Due to the existence of Pt, the separated spin-orbits of Ru $3p_{3/2}$ on PtRu/MCM-41 catalysts shifts to higher binding energy, indicating the electron loss of Ru. Since the small nanoparticles of PtRu alloy (< 4 nm), the existence of oxidation state of Pt and Ru is inevitable. The areas of Pt $4f_{7/2}$ and Ru $3p_{3/2}$ are relatively large and the binding energies of Ru 3d in all the PtRu/MCM-41 catalysts are approximately 280.0 eV (Fig. S3). This further indicates that the metal state is still dominant. Changed local environment on metal surface atoms suggests the strong electronic coupling effect

Table 1
Surface properties of PtRu/MCM-41 catalysts.

Catalysts	Loading (wt%)[a]		Chemisorption of H_2		Chemisorption of CO	
	Pt	Ru	Surface atoms (μmol/g)	Dispersion (%)	Surface atoms (μmol/g)	Dispersion (%)
Pt/MCM-41	0.7	–	18.3	50.9	13.5	37.6
$Pt_{0.8}Ru_{0.4}$/MCM-41	0.6	0.2	13.4	26.5	18.9	37.3
$Pt_{0.8}Ru_{0.8}$/MCM-41	0.7	0.6	10.6	11.1	24.7	25.9
$Pt_{0.8}Ru_{1.2}$/MCM-41	0.7	1.0	11.8	8.7	38.3	28.4
$Pt_{0.8}Ru_{1.6}$/MCM-41	0.7	1.4	15.0	8.6	42.6	24.4
Ru/MCM-41	–	1.6	6.6	4.2	39.6	25.0

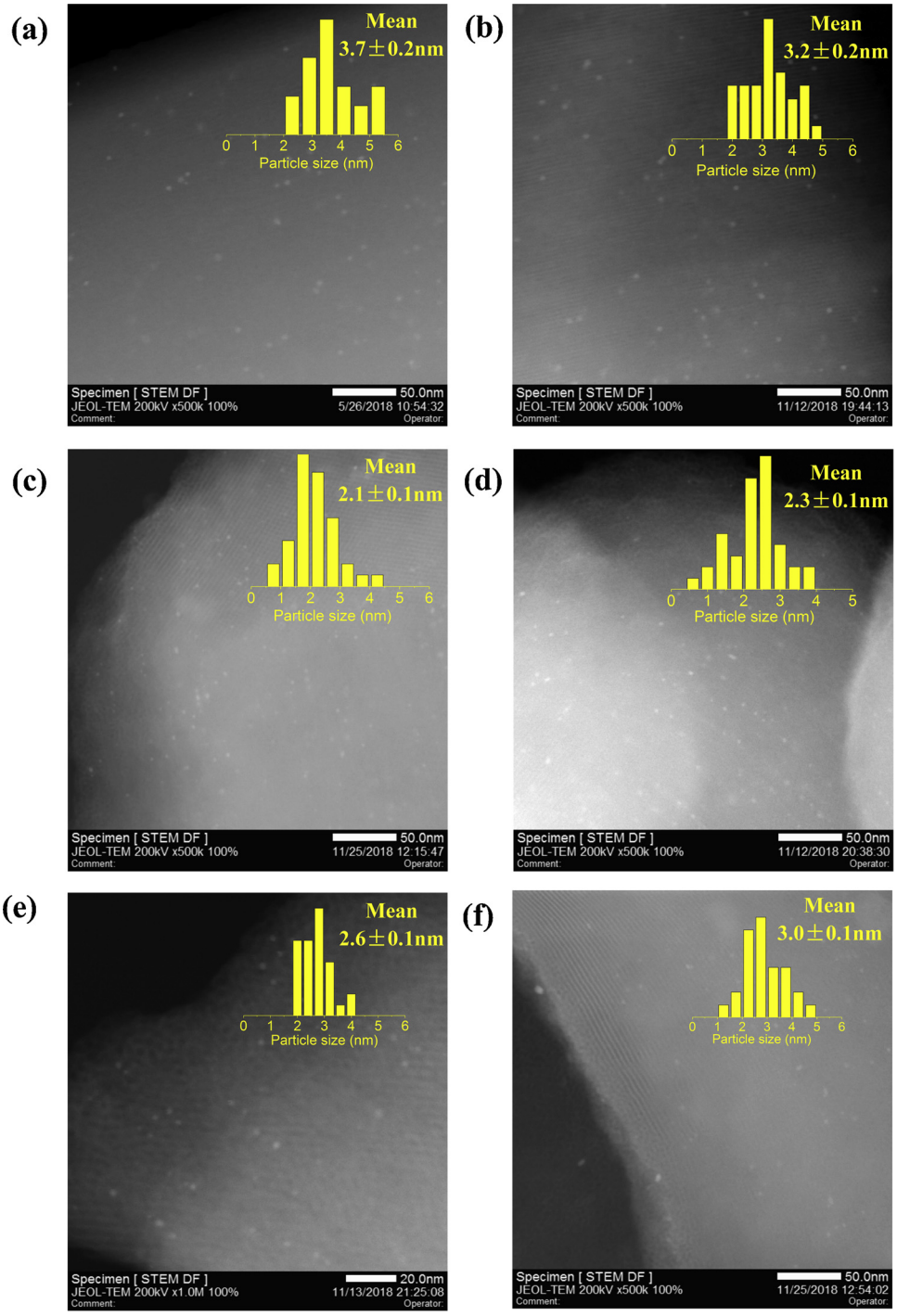

Fig. 3. HAADF-STEM images and particle size distribution of (a) Pt/MCM-41, (b) $Pt_{0.8}Ru_{0.4}$/MCM-41, (c) $Pt_{0.8}Ru_{0.8}$/MCM-41, (d) $Pt_{0.8}Ru_{1.2}$/MCM-41 (e) $Pt_{0.8}Ru_{1.6}$/MCM-41 and (f)Ru/MCM-41 catalysts.

between Pt and Ru atoms (especially on the $Pt_{0.8}Ru_{0.8}$/MCM-41 catalyst). Such changes obviously alter the electronic structures of the two metals (Pt and Ru) by orbital overlap and electronic coupling, resulting in the higher catalytic activity [59].

Moreover, DFT calculation was used to further investigate the electronic modification of the $Pt_{0.8}Ru_{0.8}$/MCM-41 catalyst as well as the interaction between GLY and metals. The Mulliken charges of pure Pt and PtRu surfaces are first investigated (Fig. 5b). In absence of Ru, the surface of Pt atoms have only a small amount of negative charge (-0.04 |e|). However, the Pt atoms on the surface of PtRu(111) are negatively charged with -0.21 |e| and the Ru atoms on the surface of PtRu(111) are positively charged with 0.12 |e|. Obviously, there is electron transfer from Ru to Pt, which is consistent with the result of XPS. It has been demonstrated that the strong adsorption of ketone intermediates could severely deactivate metal oxidation catalysts [35]. To further prove this point, the adsorption energies of GLYA on Pt(111) and PtRu(111) were calculated (Fig. S4). The results showed that the adsorption energy of GLYA on PtRu(111) (-11.20 kcal/mol) is lower than that on Pt(111) (-26.30 kcal/mol). Meanwhile, the GLYA, which is mainly adsorbed on the active sites of Ru, could be more easily desorbed from the surface of PtRu catalyst, leading to the continuous oxidation of GLY into GLYA. Therefore, the addition of Ru favors the adsorption of the reaction

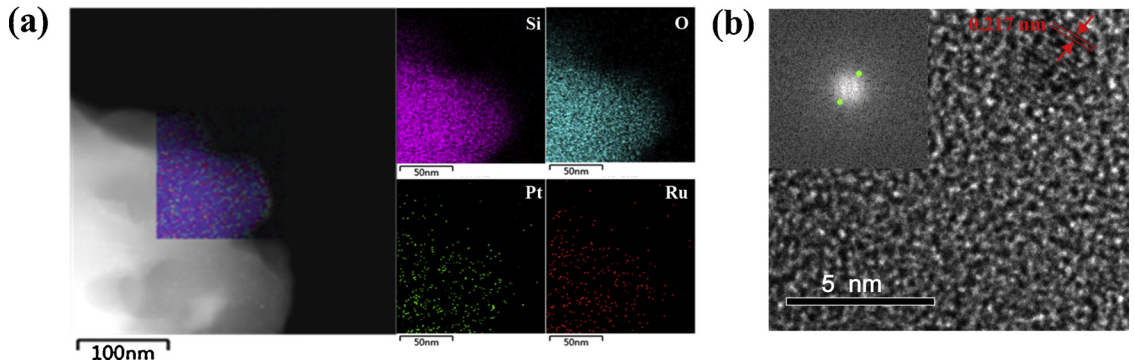

Fig. 4. (a) EDX mapping of $Pt_{0.8}Ru_{0.8}$/MCM-41 catalyst; (b) Typical shape of PtRu nanoparticles on the $Pt_{0.8}Ru_{0.8}$/MCM-41 catalyst. The inset shows FFT of the selected area and the possible PtRu shape.

intermediates with long-pair electrons such as carboxylic acid and ketone, preventing the deactivation of Pt active site [32]. Then, the *d*-partial density of states of pure Pt and PtRu surfaces are further analyzed (Fig. 5c). Compared to pure Pt(111), the number of the *d*-band peaks decreases and the *d*-bandwidth of PtRu(111) is broader, indicating a stronger delocalizability of *d* electrons. In particular, the *d*-PDOSs for the PtRu(111) surface near the Fermi level improves the catalytic activity [32]. After alloying Pt with Ru, the shifting of the *d*-band results in the stronger adsorption of GLY at Pt sites (45.39 kcal/mol) than on pure Pt (111) (41.34 kcal/mol) [Fig. 5d]. The DFT calculations further demonstrated that the interaction between Pt and Ru is critical for surface electronic configurations, which could significantly affect surface catalytic properties.

It is widely accepted that water could be facilitated to generate active hydroxyl species on Ru active sites, which subsequently oxidize C═O bound to neighboring Pt sites in the direct methanol fuel cell (DMFC) [35]. Interestingly, the catalytic activity of GLY oxidation in base-free medium was limited by the regeneration of hydroxyl groups, which is originated from the dissociation of water and molecular oxygen [11,60]. Due to the similar reaction mechanism, it is proposed that PtRu catalyst could be also beneficial to the direct reaction of molecular oxygen and water. As shown in Fig. 6, the single adsorption energies of molecular oxygen (-34.20 kcal/mol) and water (-25.36 kcal/mol) on PtRu(111) are much higher than that on Pt(111) (-17.73 and -16.10 kcal/mol, respectively), suggesting that the enhanced adsorption ability (especially molecular oxygen) may contribute to the dissociation reaction. Subsequently, we initially explored the separate dissociation of water and molecular oxygen on the Pt(111) and PtRu(111). The incorporation of Ru can greatly reduce the energy barrier of molecular oxygen dissociation (9.25 kcal/mol) [Fig. 6]. However, the activation barriers of water dissociation on the Pt(111) [19.75 kcal/mol] and PtRu (111) [19.25 kcal/mol] are almost similar. This indicates that the introduction of Ru could not promote the dissociation of water. The molecular oxygen has been proposed to participate in the catalytic cycle by regenerating hydroxide ions formed through the decomposition of a peroxide intermediate in the GLY oxidation [53]. Therefore, in addition to oxygen dissociation alone, it is highly possible that water and molecular oxygen can dissociate directly on PtRu(111) to form hydroxyl groups. DFT calculations show that the activation barriers on both Pt (111) and PtRu(111) are lower than that of separate dissociation of molecular oxygen or water. Furthermore, the activation barriers of the direct dissociation of water and molecular oxygen on PtRu(111) [5.71 kcal/mol] is significantly lower than that on Pt(111) [18.67 kcal/mol]. These further reveal that the introduction of Ru is propitious to the direct dissociation of molecular oxygen and water to hydroxyl group, leading to the enhancement of oxidation activity.

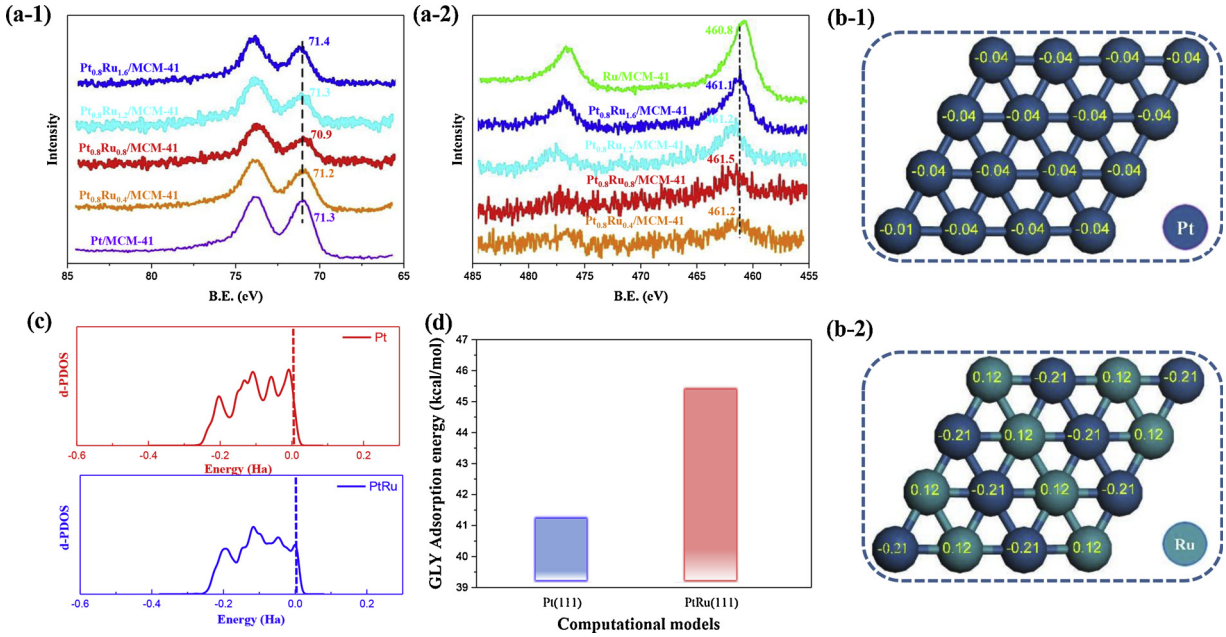

Fig. 5. (a) XPS spectra of (a-1) Pt 4*f* and (a-2) Ru 3*p* of the PtRu/MCM-41 catalysts; (b) Mulliken charge (|e|) distribution of Pt(111) and PtRu(111); (c) *d*-partial density of states of Pt(111) and PtRu(111); (d) Adsorption energy of glycerol on Pt(111) and PtRu(111).

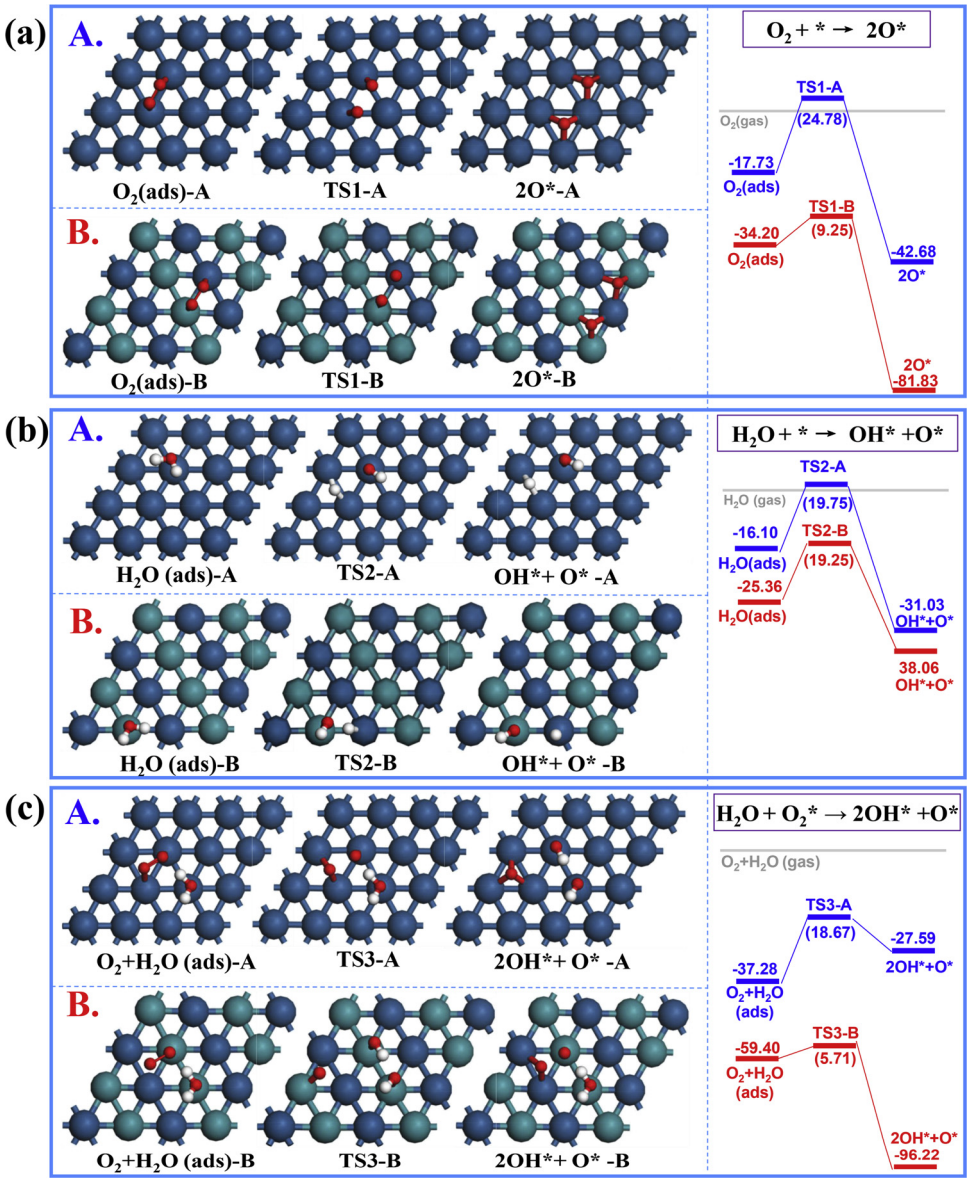

Fig. 6. The reaction mechanism for (a) dissociation of water, (b) dissociation of molecular oxygen and (c) direct dissociation of water and molecular oxygen (kcal/mol). [Blue A represents the Pt (111) model and red B represents the PtRu (111) model]. (For interpretation of the references to colour in this figure legend, the reader is referred to the web version of this article.).

Since the presence of Ru could synergistically enhance the catalytic performance of Pt catalysts, the kinetic behaviors of Pt/MCM-41 and $Pt_{0.8}Ru_{0.8}$/MCM-41 catalysts were also investigated (Fig. S5-S6 and Table S3). The reaction orders for GLY and O_2 and activation energies over Pt/MCM-41 and $Pt_{0.8}Ru_{0.8}$/MCM-41 catalysts were studied by the power function type reaction kinetic equation. The reaction orders for GLY and O_2 (0.44 and 0.27, respectively) on the $Pt_{0.8}Ru_{0.8}$/MCM-41 are lower than that on the Pt/MCM-41 catalyst (0.52 and 0.38, respectively). This indicates that the $Pt_{0.8}Ru_{0.8}$/MCM-41 catalyst has stronger adsorption ability for GLY and O_2 compared with the Pt/MCM-41 catalyst, which is consistent with the results of DFT calculation. Furthermore, glycerol oxidation on the $Pt_{0.8}Ru_{0.8}$/MCM-41 catalyst has lower activation energy (56.80 kJ/mol) than that on the Pt/MCM-41 catalyst (77.16 kJ/mol). Catalytic kinetics determination of the Pt/MCM-41 and $Pt_{0.8}Ru_{0.8}$/MCM-41 catalysts not only proves the consistency of experimental and theoretical conclusions but also provides strong evidence for the promoting role of Ru to Pt in glycerol oxidation.

3.2. Effect of Ru/Pt ratio and reaction conditions

The optimal bimetallic PtRu alloy composition (i.e., Ru/Pt ratio) was also studied to investigate synergistic effects on catalytic performance. Bimetallic PtRu/MCM-41 catalysts were synthesized with various Ru/Pt ratios and tested for oxidation of GLY in base-free medium. It is observed that synergistic effects exist within a range of Ru/Pt from 0.5 to 2.0 (mass ratio). In particular, TOFs for the $Pt_{0.8}Ru_{0.4}$/MCM-41, $Pt_{0.8}Ru_{0.8}$/MCM-41, $Pt_{0.8}Ru_{1.2}$/MCM-41, and $Pt_{0.8}Ru_{1.6}$/MCM-41 catalysts are 670.9, 823.9, 694.6 and 337.6 h^{-1}, respectively. These TOFs values are all significantly higher than those obtained on individual Pt/MCM-41 and Ru/MCM-41 catalysts under the identical reaction conditions. It has been reported that Ru/Pt atomic ratio in a range of 0.4~2.4 could enhance the glycerol binding energy [61]. The actual Ru/Pt atomic ratios of the $Pt_{0.8}Ru_{0.4}$/MCM-41 (0.93), $Pt_{0.8}Ru_{0.8}$/MCM-41 (1.4) and $Pt_{0.8}Ru_{1.2}$/MCM-41 (2.7) catalysts are related to this range (Table S1). For a more intuitive understanding of the effects of Ru/Pt ratio, the relationship between structure-sensitivity, electronic coupling effect and TOF values was shown in Fig. 7. As Ru/Pt ratio increases,

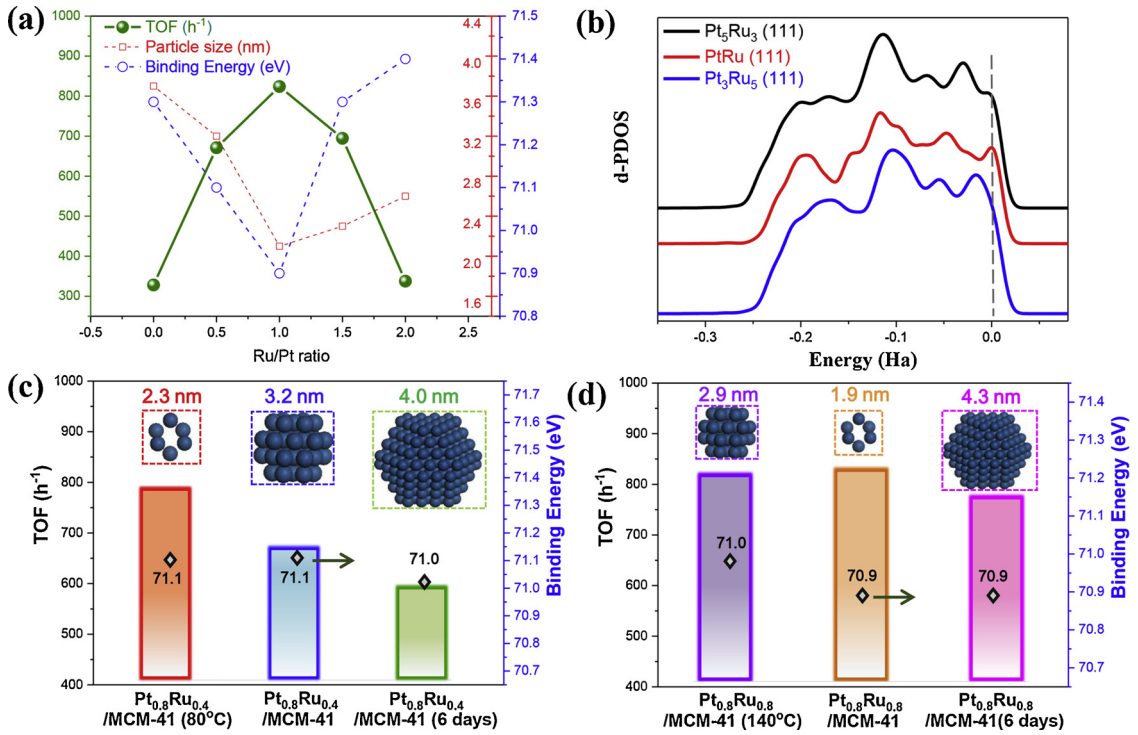

Fig. 7. (a) Effect of Ru/Pt ratio in PtRu/MCM-41 catalysts on catalytic activity during oxidation of glycerol. (b) *d*-partial density of states of Pt_5Ru_3(111), PtRu(111) and Pt_3Ru_5(111). (c) $Pt_{0.8}Ru_{0.4}$ catalysts with different particle size. (d) $Pt_{0.8}Ru_{0.8}$ catalysts with different particle size.

TOF begins to increase to 823.9 h^{-1} until Ru/Pt = 1 (Fig. 7a). Meanwhile, the particle size and binding energy (Pt $4f_{7/2}$) decrease rapidly, which indicates that both of the structure-sensitivity and electronic coupling effect play an important role in enhancing the catalytic activity at this stage. To regulate the particle size of PtRu alloy, three kinds of MCM-41 materials with different pore sizes were prepared (Fig. S7 and Table S4). Subsequently, the $Pt_{0.8}Ru_{0.4}$/MCM-41 (80 °C), $Pt_{0.8}Ru_{0.4}$/MCM-41 (140 °C) and $Pt_{0.8}Ru_{0.4}$/MCM-41 (6 days) catalysts were further investigated to confirm the co-interaction of the structure-sensitivity and electronic coupling effect, and particle size distribution and XPS spectra are provided in Fig. S8(a)-(b) and Fig. S9(a)-(b) respectively. Fig. 7c shows that the TOF of $Pt_{0.8}Ru_{0.4}$/MCM-41 (80 °C) catalyst is as high as 791.1 h^{-1} due to the small particle size (2.3 nm). The $Pt_{0.8}Ru_{0.4}$/MCM-41 (6 days) catalyst has larger particle size (4.0 nm) than $Pt_{0.8}Ru_{0.4}$/MCM-41 catalyst (3.2 nm) resulting in the lower catalytic activity (590.9 h^{-1}). Meanwhile, the binding energies of the $Pt_{0.8}Ru_{0.4}$/MCM-41 (80 °C), $Pt_{0.8}Ru_{0.4}$/MCM-41 and $Pt_{0.8}Ru_{0.4}$/MCM-41 (6 days) catalysts are similar. Thus, the enhancement of catalyst activity could be attributed to the effect of structural-sensitivity. The catalytic performance of bimetallic PtRu/MCM-41 catalysts is obviously better than that of monometallic Pt/MCM-41 catalyst. As a result, the structure-sensitivity together with electronic coupling effect improves the catalytic performance of PtRu/MCM-41 catalysts until Pt/Ru = 1.

However, when Ru/Pt ratio is higher than 1, TOF decreases rapidly (Fig. 7a). The large nanoparticle is no longer the main factor because the slope of particle size curve is low. The binding energy still increases rapidly, suggesting that the electronic coupling effect is the dominant factor. To further prove this point, the $Pt_{0.8}Ru_{0.8}$/MCM-41 (140 °C) and $Pt_{0.8}Ru_{0.8}$/MCM-41 (6 days) catalysts were analysed. The particle sizes of the $Pt_{0.8}Ru_{0.8}$/MCM-41 (140 °C) and $Pt_{0.8}Ru_{0.8}$//MCM-41 (6 days) catalysts are 2.9 and 4.3 nm, respectively [Fig. S8(c)-(d)]. The binding energies (Pt $4f_{7/2}$) of the two catalysts are very similar to that of $Pt_{0.8}Ru_{0.8}$/MCM-41 catalyst (70.9 eV) [Fig. S9(c)-(d)]. As shown in Fig. 7d, although the particle size of $Pt_{0.8}Ru_{0.8}$/MCM-41 (140 °C) catalyst (2.9 nm) is larger than that of the $Pt_{0.8}Ru_{0.8}$/MCM-41 catalyst (1.9 nm), $Pt_{0.8}Ru_{0.8}$/MCM-41 (140 °C) catalyst exhibits approximately same catalytic activity (TOF: 810.5 h^{-1}) as $Pt_{0.8}Ru_{0.8}$/MCM-41 catalyst (TOF: 823.9 h^{-1}). This further demonstrates that the electronic coupling effect is the main factor affecting the catalytic activity with Ru/Pt ≥ 1. For the $Pt_{0.8}Ru_{0.8}$/ MCM-41 (6 days) catalyst, the TOF (744.3 h^{-1}) is only a little lower than that of $Pt_{0.8}Ru_{0.8}$/MCM-41 catalyst due to the larger particle size, but it is still higher than that of other catalysts ($Pt_{0.8}Ru_{0.4}$/MCM-41, $Pt_{0.8}Ru_{1.2}$/MCM-41 and $Pt_{0.8}Ru_{1.6}$/MCM-41 catalysts). This indicates that the electronic coupling effect was of great importance to affect the catalytic activity compared with structure sensitivity. Furthermore, from the perspective of bimetallic ratio, excessive Ru (Ru/Pt > 1) decreases the proportion of Pt active sites on the surface (H_2-TPD and CO-TPD) and weakens the electronic coupling effect between Pt and Ru (H_2-TPR and XPS), leading to the poor catalytic activity. Therefore, only the appropriate PtRu ratio could enhance the catalytic activity.

Essentially, the volcanic relationship between TOF and Ru/Pt ratio is mainly due to the structure-sensitivity and electronic coupling effect. In terms of structural-sensitivity, the incorporation of appropriate Ru enhances the dispersion of PtRu alloy nanoparticles. In contrast, excessive Ru increases the Pt loadings resulting in the larger particle size. Therefore, structural-sensitivity plays an important role in improving the catalytic activity only when Ru/Pt ratio is less than 1. However, the electronic coupling effect has a great influence on the catalytic activity all along the Ru/Pt ratio. The binding energy (Pt $4f_{7/2}$) decreases first and then increases with the Ru/Pt ratio. Similar results have also been found in other literatures, but no specific explanation has been given [62,63]. Three calculation models with different Ru/Pt ratios [Pt_5Ru_3(111), PtRu(111) and Pt_3Ru_5(111)] were further used to investigate the changes in electronic properties caused by different proportions of Pt and Ru (Fig. 7b). Obviously, too much or too little Ru results in the *d*-PDOSs far away from Fermi level. Only when the molar ratio of Pt to Ru is 1:1, the significant increase of *d*-PDOS near the Fermi enhances the catalytic activity with the strongest electronic coupling effect between Ru and Pt. The optimum Ru/Pt molar ratio in the experiment ($Pt_{0.8}Ru_{0.8}$/MCM-41 catalyst) is 1.4 corresponding to Ru/Pt

mass ratio equal to 1.33 (all the actual ratios determined by ICP). This shows that there is a gap between the experimental and theoretical values. The complete 1:1 PtRu alloy model is selected in the theoretical calculation. However, it is difficult to form complete 1:1 alloy nanoparticles on the basis of the feed composition. Due to the uniform distribution of Ru compared to Pt, it is necessary to add more Ru than Pt in order to form more PtRu alloy nanoparticles with molar ratio of 1. Therefore, $Pt_{0.8}Ru_{0.8}$/MCM-41 catalyst (Ru/Pt molar ratio = 1.4) exhibited the strongest electron coupling effect with excellent catalytic activity (TOF: 823.9 h^{-1}).

The relationship between Ru/Pt ratio and the selectivity of products was further investigated (Table S5). Before Ru/Pt ratio is less than 1, the selectivity of GLYA increases, and the selectivity of intermediate GLYAD and GLYOA decrease. It indicates that the incorporation of Ru could significantly improve the selectivity of GLYA and inhibit C—C bond breaking to produce other by-products. 74.1% GLYA selectivity is obtained on the $Pt_{0.8}Ru_{0.8}$/MCM-41 catalyst (Ru/Pt = 1). When Ru/Pt ratio is higher than 1, the selectivity of GLYAD increases, while the selectivity of GLYA and GLYOA decreases. This could be attributed to the higher Ru loading which covers the active sites of Pt and decreases the oxidation depth.

The catalytic performance of the optimum $Pt_{0.8}Ru_{0.8}$/MCM-41 catalyst is tested at different reaction temperatures (Fig. 8a).The conversion of GLY increases with reaction temperature. The selectivity of GLYAD, GLYA and DHA decreases as reaction temperature increases from 80 °C to 100 °C due to the increase of oxidation depth [12]. Fig. 8b shows the conversion/selectivity-time profiles at 80 °C. With the prolongation of reaction time, the selectivity of initial oxidation products (GLYAD and DHA) decreases. The selectivity of GLYA reaches its maximum (80.1%) at 12 h. Thus, under the optimized conditions (80 °C, 1 MPa O_2 and 12 h), the conversion of GLY is 78.2% and the selectivity of GLYA is as high as 80.1% with the TOF of 823.9 h^{-1}. It is worth noted that the conversion of GLY increases almost linearly with the prolongation of reaction time. This indicates that the catalyst still remains good catalytic activity in the reaction process. In the previous work, the oxidation reaction appeared to be inhibited by the products (such as GLYA) formed during oxidation, preventing further improvement of reaction conversion [37]. However, there is no similar phenomenon on the $Pt_{0.8}Ru_{0.8}$/MCM-41 catalyst. It has been reported that the bimetallic PtRu catalysts display the enhancement of CO-poisoning tolerance in the DMFC reaction. Koper et al. [31] demonstrated that the incorporation of Ru to Pt weakens the adsorption of both CO and OH on the Pt sites, while the adsorption of these species on the Ru sites is strengthened. Therefore, we infer that the as-formed GLYA could adsorb on the Ru active site in the reaction process, and the active sites of Pt still further catalyze GLY, so that the catalyst still remains superior catalytic activity. The catalyst stability was further studied by recycling the used $Pt_{0.8}Ru_{0.8}$/MCM-41 catalyst for 5 runs (Fig. S10). The $Pt_{0.8}Ru_{0.8}$/MCM-41 catalyst is still very stable with 68.7% conversion of GLY at the 5th run, indicating that the $Pt_{0.8}Ru_{0.8}$/MCM-41 catalyst has good stability. The used $Pt_{0.8}Ru_{0.8}$/MCM-41 catalyst was further characterized (Fig. S11, Fig. S12 and Table S6). XPS result shows that Ru exists as a stable metal state in the oxidation reaction. Although the particle size of the used $Pt_{0.8}Ru_{0.8}$/MCM-41 catalyst increased (from 2.1 nm to 3.5 nm) [Fig. S12], it has been demonstrated that the increase of particle size is no longer the main factor affecting the catalytic performance at Ru/Pt = 1 (Fig. 7). And there is negligible Pt and Ru leaching during reaction (Table S6). All these indicate that the $Pt_{0.8}Ru_{0.8}$/MCM-41 catalyst is a stable catalyst for glycerol oxidation in base-free medium.

A comparison of the catalytic performance between the $Pt_{0.8}Ru_{0.8}$/MCM-41 catalyst and other reported bimetallic catalysts is given in Table 2. 2%Pt_9Sn_1/C–R and 5%PtCu/C catalysts exhibit high catalytic conversion because of their high noble metal loading. However, the TOFs and the selectivity of GLYA are not very high. Obviously, the $Pt_{0.8}Ru_{0.8}$/MCM-41 catalyst shows high TOF due to its small particle size and strong electron coupling effect. Importantly, the selectivity of GLYA is also increased to more than 80%. This PtRu catalyst synthesized herein gives a reference for designing stable and efficient bimetallic catalysts for glycerol oxidation.

3.3. Plausible reaction pathways and mechanism

The oxidation mechanism on the $Pt_{0.8}Ru_{0.8}$/MCM-41 catalyst can be summarized in Fig. 9. The generation of GLYA requires the selective oxidation of primary alcohol of GLY to first produce GLYAD. Subsequently, GLYAD is oxidized to GLYA. Due to the addition of Ru, there is a strong interaction between Pt and Ru atoms, resulting in the electron enrichment on Pt surface. The strong electronic coupling effect on the $Pt_{0.8}Ru_{0.8}$/MCM-41 catalyst promotes the direct dissociation of molecular oxygen and water to OH group, leading to the excellent catalytic activity. Meanwhile, the improved selectivity of GLYA and stability are attributed to weak adsorption of GLYA on the surface of PtRu alloy nanoparticle. Ultimately, the $Pt_{0.8}Ru_{0.8}$/MCM-41 catalyst displays excellent catalytic performance.

4. Conclusions

In this paper, we explored a new strategy to simultaneously improve the catalytic activity and stability by synthesizing PtRu/MCM-41 catalyst, and the potential structure-performance relationship is systematically investigated. The incorporation of Ru effectively enhances the

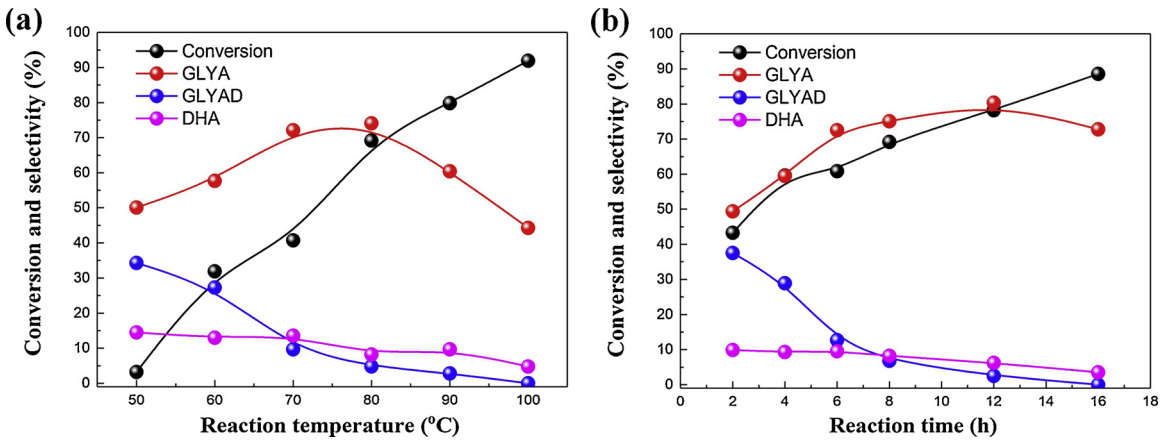

Fig. 8. Glycerol conversion and selectivity on the $Pt_{0.8}Ru_{0.8}$/MCM-41 catalyst as a function of (a) Reaction temperature (reaction condition: 0.2 catalyst, 25 mL aqueous solution of glycerol (0.22 M), MPa O_2, 8 h) and (b) Reaction time (reaction condition: 0.2 catalyst, 25 mL aqueous solution of glycerol (0.22 M), 80 °C, 1 MPa O_2).

Table 2
Oxidation of glycerol over the $Pt_{0.8}Ru_{0.8}$/MCM-41 catalyst and other reported bimetallic catalysts[a].

Catalyst	Selectivity (%)				Conversion (%)	TOF (h^{-1})	Reference
	GLYAD	GLYA	DHA	GLYOA			
$Pt_{0.8}Ru_{0.8}$/MCM-41	2.5	80.4	6.2	3.9	78.2	823.9	This work
2%Pt_9Sn_1/C-R[b]	1.1	55.4	7.2	8.0	91.1	113.0	[8]
1%Au_1Pt_3/MgO[c]	–	72.2	–	3.3	42.9	107.0	[64]
5%PtCu/C[d]	1.5	70.8	10.1	9.2	86.2	–	[30]
1% Au − Pt − Pd/TiO_2 [e]	–	55.0	–	7.0	37.0	378.0	[65]

a. Reaction conditions: glycerol/Pt molar ratio 700, 80℃, 1 MPa O_2, 12 h;.
b. Reaction conditions: glycerol/Pt molar ratio 1000, 60℃, Oxygen flow (15 mL/min), 8 h;.
c. Reaction conditions: glycerol/Pt molar ratio 1000, 60℃, 1 MPa O_2, 4 h;.
d. Reaction conditions: glycerol/Pt molar ratio 500, 60℃, Oxygen flow (150 mL/min), 6 h;.
e. Reaction conditions: glycerol/Au molar ratio 2728, 100℃, 4 h.

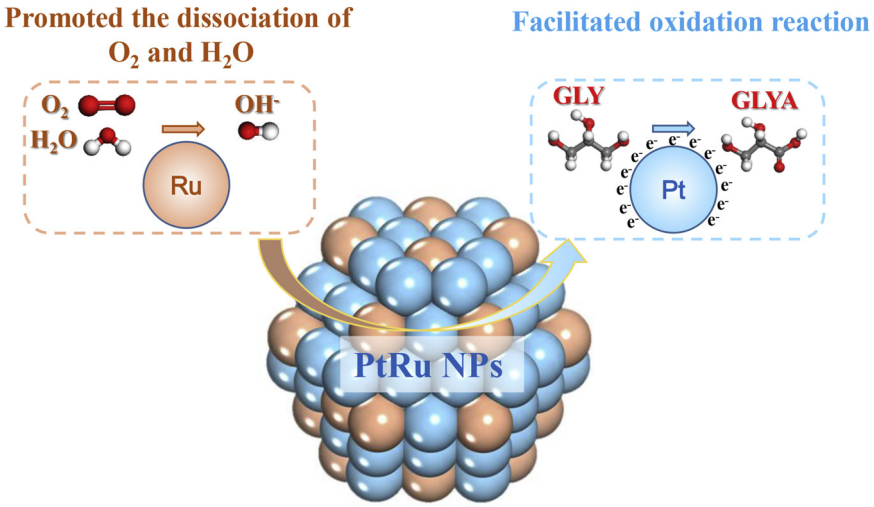

Fig. 9. Plausible oxidation mechanism on the $Pt_{0.8}Ru_{0.8}$/MCM-41 catalyst.

dispersion of PtRu nanoparticles (ca. 1.9 nm) on the MCM-41. The resultant PtRu nanoparticles, in the form of alloy, lead to upsurge of TOF and selectivity of glyceric acid. In addition, the PtRu catalysts show strong interaction between Pt and Ru and facilitate electron transfer from Ru to Pt. DFT calculation further demonstrated that the PtRu catalysts could be beneficial to the direct dissociation of molecular oxygen and water to hydroxyl group. Moreover, the TOF increases with the Ru/Pt ratio to a maximum value of 823.9 h^{-1} at the Ru/Pt ratio of 1:1 followed by a decline in activity. Under the optimized conditions (80 °C, 1 MPa O_2 and 12 h), the conversion of GLY is 78.2% and the selectivity of GLYA is as high as 80.1% with the TOF of 823.9 h^{-1}.

Declaration of Competing Interest

The authors declare that they have no known competing financial interests or personal relationships that could have appeared to influence the work reported in this paper.

Acknowledgments

Our work was supported by the National Science Foundation of China (Grant No. 21606254, 21776312 and 21706290), Fundamental Research Funds for the Central Universities (18CX02130A, 18CX06067A and 18CX02014A), Independent innovation foundation of Qingdao (17-1-1-18-jch), Postgraduate Innovation Engineering (YCX2019030), Shandong Key R&D Program (2018GGX107005) and Natural Science Foundation of Shandong Province (ZR2017MB004).

Appendix A. Supplementary data

Supplementary material related to this article can be found, in the online version, at doi:https://doi.org/10.1016/j.apcatb.2019.118070.

References

[1] T. Gao, J. Chen, W. Fang, Q. Cao, W. Su, F. Dumeignil, Ru/$Mn_XCe_1O_Y$ catalysts with enhanced oxygen mobility and strong metal-support interaction: exceptional performances in 5-hydroxymethylfurfural base-free aerobic oxidation, J. Catal. 368 (2018) 53–68.
[2] G.L. Caneppele, T.S. Almeida, C.R. Zanata, É. Teixeira-Neto, P.S. Fernández, G.A. Camara, C.A. Martins, Exponential improving in the activity of Pt/C nanoparticles of glycerol electrooxidation by Sb ad-atoms deposition, Appl. Catal. B 200 (2017) 114–120.
[3] R. Lucchetti, L. Onotri, L. Clarizia, F.D. Natale, I.D. Somma, R. Andreozzi, R. Marotta, Removal of nitrate and simultaneous hydrogen generation through photocatalytic reforming of glycerol over “in situ” prepared zero-valent nano copper/P25, Appl. Catal. B 202 (2017) 539–549.
[4] N. Yan, X. Chen, Sustainability: don’t waste seafood waste, Nature 524 (2015) 155–157.
[5] Y. Sun, X. Li, J. Wang, W. Ning, J. Fu, X. Lu, Z. Hou, Carbon film encapsulated Pt NPs for selective oxidation of alcohols in acidic aqueous solution, Appl. Catal. B 218 (2017) 538–544.
[6] N. Yan, Y. Wang, Catalyst: is the amino acid a new frontier for biorefineries? Chem 5 (4) (2019) 739–741.
[7] Y. Wang, S. Furukawa, Z. Zhang, L. Torrente-Murciano, S.A. Khan, N. Yan, Oxidant free conversion of alcohols to nitriles over Ni-based catalysts, Catal. Sci. Technol. 9 (2019) 86–96.
[8] J. Dou, B. Zhang, H. Liu, J. Hong, S. Yin, Y. Huang, R. Xu, Carbon supported Pt_9Sn_1 nanoparticles as an efficient nanocatalyst for glycerol oxidation, Appl. Catal. B 180 (2016) 78–85.
[9] P. Sudarsanam, E. Peeters, E.V. Makshina, V.I. Parvulescu, B.F. Sels, Advances in porous and nanoscale catalysts for viable biomass conversion, Chem. Soc. Rev. 48 (8) (2019) 2366–2421.

[10] S. Liu, K. Sun, B. Xu, Specific selectivity of Au-Catalyzed oxidation of glycerol and other C3-Polyols in water without the presence of a base, ACS Catal. 4 (2014) 2226–2230.

[11] H. Yan, H. Qin, X. Feng, X. Jin, W. Liang, N. Sheng, C. Zhu, H. Wang, B. Yin, Y. Liu, X. Chen, C. Yang, Synergistic Pt/MgO/SBA-15 nanocatalysts for glycerol oxidation in base-free medium: catalyst design and mechanistic study, J. Catal. 370 (2019) 434–446.

[12] L. Tao, B. Yan, Y. Liang, B. Xu, Sustainable production of acrolein: catalytic performance of hydrated tantalum oxides for gas-phase dehydration of glycerol, Green Chem. 15 (2013) 696.

[13] E. Maris, R. Davis, Hydrogenolysis of glycerol over carbon-supported Ru and Pt catalysts, J. Catal. 249 (2007) 328–337.

[14] F. Wang, S. Shao, C. Liu, C. Xu, R. Yang, W. Dong, Selective oxidation of glycerol over Pt supported on mesoporous carbon nitride in base-free aqueous solution, Chem. Eng. J. 264 (2015) 336–343.

[15] G.M. Lari, C. Mondelli, J. Pérez-Ramírez, Gas-phase oxidation of glycerol to dihydroxyacetone over tailored iron zeolites, ACS Catal. 5 (2015) 1453–1461.

[16] W. Hu, D. Knight, B. Lowry, A. Varma, Selective oxidation of glycerol to dihydroxyacetone over Pt-Bi/C catalyst: optimization of catalyst and reaction conditions, Ind. Eng. Chem. Res. 49 (2010) 10876–10882.

[17] Y. Xiao, J. Greeley, A. Varma, Z. Zhao, G. Xiao, An experimental and theoretical study of glycerol oxidation to 1, 3-dihydroxyacetone over bimetallic Pt-Bi catalysts, AIChE J. 63 (2017) 705–715.

[18] X. Ning, Y. Li, H. Yu, F. Peng, H. Wang, Y. Yang, Promoting role of bismuth and antimony on Pt catalysts for the selective oxidation of glycerol to dihydroxyacetone, J. Catal. 335 (2016) 95–104.

[19] S. Hirasawa, H. Watanabe, T. Kizuka, Y. Nakagawa, K. Tomishige, Performance, structure and mechanism of Pd–Ag alloy catalyst for selective oxidation of glycerol to dihydroxyacetone, J. Catal. 300 (2013) 205–216.

[20] C. Xu, Y. Du, C. Li, J. Yang, G. Yang, Insight into effect of acid/base nature of supports on selectivity of glycerol oxidation over supported Au-Pt bimetallic catalysts, Appl. Catal. B 164 (2015) 334–343.

[21] B. Katryniok, H. Kimura, E. Skrzyńska, J. Girardon, P. Fongarland, M. Capron, R. Ducoulombier, N. Mimura, S. Paul, F. Dumeignil, Selective catalytic oxidation of glycerol: perspectives for high value chemicals, Green Chem. 13 (2011) 1960.

[22] J. Lei, H. Dong, X. Duan, W. Chen, G. Qian, D. Chen, X. Zhou, Insights into activated carbon-supported platinum catalysts for base-free oxidation of glycerol, Ind. Eng. Chem. Res. 55 (2016) 420–427.

[23] L.S. Ribeiro, E.G. Rodrigues, J.J. Delgado, X. Chen, M.F.R. Pereira, J.J.M. Órfão, Pt, and Pt-Cu catalysts supported on Carbon Nanotube (CNT) for the selective oxidation of glycerol in alkaline and base-free conditions, Ind. Eng. Chem. Res. 55 (2016) 8548–8556.

[24] M. Zhang, J. Shi, W. Ning, Z. Hou, Reduced graphene oxide decorated with PtCo bimetallic nanoparticles: facile fabrication and application for base-free oxidation of glycerol, Catal. Today 298 (2017) 234–240.

[25] M. Zhang, R. Nie, L. Wang, J. Shi, W. Du, Z. Hou, Selective oxidation of glycerol over carbon nanofibers supported Pt catalysts in a base-free aqueous solution, Catal. Commun. 59 (2015) 5.

[26] D. Liang, J. Gao, H. Sun, P. Chen, Z. Hou, X. Zheng, Selective oxidation of glycerol with oxygen in a base-free aqueous solution over MWNTs supported Pt catalysts, Appl. Catal. B 106 (2011) 423–432.

[27] D. Liang, J. Gao, J. Wang, P. Chen, Z. Hou, X. Zheng, Selective oxidation of glycerol in a base-free aqueous solution over different sized Pt catalysts, Catal. Commun. 10 (2009) 1586–1590.

[28] Y. Shen, S. Zhang, H. Li, Y. Ren, H. Liu, Efficient synthesis of lactic acid by aerobic oxidation of glycerol on Au–Pt/TiO2 catalysts[J], Chem. Eur. J. 16 (25) (2010) 7368–7371.

[29] A. Iriondo, J.F. Cambra, V.L. Barrio, M.B. Guemez, P.L. Arias, M.C. Sanchez-Sanchez, R.M. Navarro, J.L.G. Fierro, Glycerol liquid phase conversion over monometallic and bimetallic catalysts: effect of metal, support type and reaction temperatures, Appl. Catal. B 106 (2011) 83–93.

[30] D. Liang, J. Gao, J. Wang, P. Chen, Y. Wei, Z. Hou, Bimetallic Pt-Cu catalysts for glycerol oxidation with oxygen in a base-free aqueous solution, Catal. Commun. 12 (2011) 1059–1062.

[31] L.E. Chinchilla, C.M. Olmos, A. Villa, A. Carlsson, L. Prati, X. Chen, G. Blanco, J.J. Calvino, A.B. Hungría, Ru-modified Au catalysts supported on ceria–zirconia for the selective oxidation of glycerol, Catal. Today 253 (2015) 178–189.

[32] L. Zhao, S. Wang, Q. Ding, W. Xu, P. Sang, Y. Chi, X. Lu, W. Guo, The oxidation of methanol on PtRu (111): a periodic density functional theory investigation, J. Phys. Chem. C 119 (2015) 20389–20400.

[33] H. Liu, N. Tian, M.P. Brandon, Z. Zhou, J. Lin, C. Hardacre, W. Lin, S. Sun, Tetrahexahedral Pt nanocrystal catalysts decorated with Ru adatoms and their enhanced activity in methanol electrooxidation, ACS Catal. 2 (2012) 708–715.

[34] H.J. Kim, S.M. Choi, S. Green, G.A. Tompsett, S.H. Lee, G.W. Huber, W.B. Kim, Highly active and stable PtRuSn/C catalyst for electrooxidations of ethylene glycol and glycerol, Appl. Catal. B 101 (2011) 366–375.

[35] A. Serov, C. Kwak, Recent achievements in direct ethylene glycol fuel cells (DEGFC), Appl. Catal. B 97 (2010) 1–12.

[36] M.T.M. Koper, T.E. Shubina, R.A. van Santen, Periodic density functional study of CO and OH adsorption on Pt-Ru alloy surfaces: implications for CO tolerant fuel cell catalysts, J. Phys. Chem. B 106 (2002) 686–692.

[37] B.N. Zope, R.J. Davis, Inhibition of gold and platinum catalysts by reactive intermediates produced in the selective oxidation of alcohols in liquid water, Green Chem. 13 (2011) 3484.

[38] K.M. Parida, S.S. Dash, S. Singha, Structural properties and catalytic activity of Mn-MCM-41 mesoporous molecular sieves for single-step amination of benzene to aniline, Appl. Catal. A Gen. 351 (2008) 59–67.

[39] A. Corma, Q. Kan, M.T. Navarro, J. Pérez-Pariente, F. Rey, Synthesis of MCM-41 with different pore diameters without addition of auxiliary organics, Chem. Mater. 9 (1997) 2123–2126.

[40] B. Delley, From molecules to solids with the $DMol^3$ approach, J. Chem. Phys. 113 (2000) 7756–7764.

[41] X. Feng, J. Yang, X. Duan, Y. Cao, B. Chen, W. Chen, D. Lin, G. Qian, D. Chen, C. Yang, X. Zhou, Enhanced catalytic performance for propene epoxidation with H_2 and O_2 over bimetallic Au–Ag/Uncalcined titanium Silicate-1 catalysts, ACS Catal. (2018).

[42] R. García-Muelas, Q. Li, N. López, Density functional theory comparison of methanol decomposition and reverse reactions on metal surfaces, ACS Catal. 5 (2015) 1027–1036.

[43] S. Zhang, H. Yan, M. Wei, D.G. Evans, X. Duan, Hydrogenation mechanism of carbon dioxide and carbon monoxide on Ru (0001) surface: a density functional theory study, RSC Adv. 4 (2014) 30241.

[44] D.J. Chadi, Special points for Brillouin-zone integrations, Phys. Rev. B 16 (1977) 1746–1747.

[45] T.A. Halgren, The synchronous-transit method for determining reaction pathways and locating molecular transition states, Chem. Phys. Lett. 49 (1977) 225–232.

[46] H. Yan, X. Feng, Y. Liu, C. Yang, H. Shan, Catalytic cracking of acetic acid and its ketene intermediate over HZSM-5 catalyst: a density functional theory study, Mol. Catal. 437 (2017) 11–17.

[47] J.L. Gómez De La Fuente, M.V. Martínez-Huerta, S. Rojas, P. Hernández-Fernández, P. Terreros, J.L.G. Fierro, M.A. Peña, Tailoring and structure of PtRu nanoparticles supported on functionalized carbon for DMFC applications: new evidence of the hydrous ruthenium oxide phase, Appl. Catal. B 88 (2009) 505–514.

[48] P. Panagiotopoulou, J. Papavasiliou, G. Avgouropoulos, T. Ioannides, D.I. Kondarides, Water–gas shift activity of doped Pt/CeO_2 catalysts, Chem. Eng. J. 134 (2007) 16–22.

[49] I. Gandarias, P.L. Arias, J. Requies, M.B. Güemez, J.L.G. Fierro, Hydrogenolysis of glycerol to propanediols over a Pt/ASA catalyst: the role of acid and metal sites on product selectivity and the reaction mechanism, Appl. Catal. B Environ. 97 (2010) 248–256.

[50] Y.J. Zhang, A. Maroto-Valiente, I. Rodriguez-Ramos, Q. Xin, A. Guerrero-Ruiz, Synthesis and characterization of carbon black supported Pt–Ru alloy as a model catalyst for fuel cells, Catal. Today 94 (2004) 619–626.

[51] A. Guerrero-Ruiz, P. Badenes, I. Rodríguez-Ramos, Study of some factors affecting the Ru and Pt dispersions over high surface area graphite-supported catalysts, Appl. Catal. A 173 (1998) 313–321.

[52] M. Uchida, A.T. Bell, A study of NO reduction by H_2 over an alumina-supported ruthenium catalyst, J. Catal. 60 (1979) 204–215.

[53] X. Jin, C. Zeng, W. Yan, M. Zhao, P. Bobba, H. Shi, P.S. Thapa, B. Subramaniam, R.V. Chaudhari, Lattice distortion induced electronic coupling results in exceptional enhancement in the activity of bimetallic PtMn nanocatalysts, Appl. Catal. A 534 (2017) 46–57.

[54] S.L. Zhao, H.J. Yin, L. Du, G.P. Yin, Z.Y. Tang, S.Q. Liu, Three dimensional N-Doped Graphene/PtRu nanoparticle hybrids as high performance anode for direct methanol fuel cells, J. Mater. Chem. A 2 (2014) 3719–3724.

[55] X. Jin, M. Zhao, W. Yan, C. Zeng, P. Bobba, P.S. Thapa, B. Subramaniam, R.V. Chaudhari, Anisotropic growth of PtFe nanoclusters induced by lattice-mismatch: efficient catalysts for oxidation of biopolyols to carboxylic acid derivatives, J. Catal. 337 (2016) 272–283.

[56] X.F. Shen, L.J. Garces, Y.S. Ding, K. Laubernds, R.P. Zerger, M. Aindow, E.J. Neth, S.L. Suib, Behavior of H_2 chemisorption on Ru/TiO_2 surface and its application in evaluation of Ru particle sizes compared with TEM and XRD analyses, Appl. Catal. A 335 (2008) 187.

[57] E. Antolini, F. Cardellini, Formation of carbon supported PtRu alloys: an XRD analysis, J. Alloys. Compd. 315 (2001) 118–122.

[58] H. Song, J. Wang, Z. Wang, H. Song, F. Li, Z. Jin, Effect of titanium content on dibenzothiophene HDS performance over Ni_2P/Ti-MCM-41 catalyst, J. Catal. 311 (2014) 257–265.

[59] X. Jin, H. Yan, C. Zeng, P.S. Thapa, B. Subramaniam, R.V. Chaudhari, Phase transformed PtFe nanocomposites show enhanced catalytic performances in oxidation of glycerol to tartronic acid, Ind. Eng. Chem. Res. 56 (2017) 13157–13164.

[60] B.N. Zope, D.D. Hibbitts, M. Neurock, R.J. Davis, Reactivity of the gold/water interface during selective oxidation catalysis, Science 330 (2010) 74–78.

[61] Y. Kim, H.W. Kim, S. Lee, J. Han, D. Lee, J.-R. Kim, T.-W. Kim, C.-U. Kim, S.-Y. Jeong, H.-J. Chae, The role of ruthenium on carbon-supported PtRu catalysts for electrocatalytic glycerol oxidation under acidic conditions, ChemCatChem 9 (2017) 1683–1690.

[62] F. Richarz, B. Wohlmann, U. Vogel, H. Hoffschulz, K. Wandelt, Surface and electrochemical characterization of electrodeposited PtRu alloys, Surf. Sci. 335 (1995) 361–371.

[63] M. Hyun, S. Kim, B. Lee, D. Peck, Y. Shul, D. Jung, Effect of $NaBH_4$ concentration on the characteristics of PtRu/C catalyst for the anode of DMFC prepared by the impregnation method, Catal. Today 132 (2008) 138–145.

[64] G.L. Brett, Q. He, C. Hammond, P.J. Miedziak, N. Dimitratos, M. Sankar, A.A. Herzing, M. Conte, J.A. Lopez-Sanchez, C.J. Kiely, D.W. Knight, S.H. Taylor, G.J. Hutchings, Selective oxidation of glycerol by highly active bimetallic catalysts at ambient temperature under base-free conditions, Angew. Chem. Int. Ed. 50 (2011) 10136–10139.

[65] S.A. Kondrat, P.J. Miedziak, M. Douthwaite, G.L. Brett, T.E. Davies, D.J. Morgan, J.K. Edwards, D.W. Knight, C.J. Kiely, S.H. Taylor, G.J. Hutchings, Base-free oxidation of glycerol using titania-supported trimetallic Au-Pd-Pt nanoparticles, ChemSusChem 7 (2014) 1326–1334.